GODDARD

NGL-05-002-105

SPALL VELOCITY MEASUREMENTS FROM LABORATORY IMPACT CRATERS

IN-46-CR

217442

44P

Carol A. Polanskey and Thomas J. Ahrens

Division of Geological and Planetary Sciences
California Institute of Technology
Pasadena, California 91125

Submitted to *Icarus*

(NASA-CR-185364) SPALL VELOCITY MEASUREMENTS FROM LABORATORY IMPACT CRATERS (California Inst. of Tech.) 44 p CSCL 08G
N89-26303
Unclas
G3/46 0217442

Number of Manuscript Pages: 44

Number of Figures: 9

Number of Tables: 1

Contribution number 4405 from the Division of Geological and Planetary Sciences, California Institute of Technology, Pasadena, California, 91125

Proposed Running Head: Spall Velocity Measurements

Please direct all correspondence to:

Carol A. Polanskey
Caltech 170-25
Pasadena, CA 91125

ABSTRACT

Spall velocities were measured for a series of impacts into San Marcos gabbro. Impact velocities ranged from 1 to 6.5km/sec. Projectiles varied in material and size with a maximum mass of 4g for a lead bullet to a minimum of 0.04g for an aluminium sphere. The spall velocities were calculated both from measurements taken from films of the events and from estimates based on range measurements of the spall fragments. The maximum spall velocity observed was 27m/sec, or 0.5 percent of the impact velocity.

The measured spall velocities were within the range predicted by the Melosh (1984) spallation model for the given experimental parameters. The compatability between the Melosh model for large planetary impacts and the results of these small scale experiments is considered in detail.

The targets were also bisected to observe the internal fractures. A series of fractures were observed whose location coincided with the boundary of the theoretical near surface zone predicted by Melosh. Above this boundary the target material should receive reduced levels of compressive stress as compared to the more highly shocked region below.

INTRODUCTION

In this paper we present results of experiments designed to constrain theories of spallation in high velocity impacts. Spallation, or the separation of large fragments from a free surface as a result of dynamic tensile failure, is of interest as a means of ejecting lightly shocked material from planetary and asteroidal surfaces.

Much of the recent interest in spallation has resulted from the discovery that the SNC meteorites (shergottites, nakhlites, and Chassigny) possibly originated on Mars (McSween and Stopler, 1980; Wood and Ashwal, 1981). The low levels of shock damage found in several of these meteorites has motivated a search for mechanisms capable of accelerating ejecta to planetary escape velocities without subjecting them to intense shock pressure. This is a problem because for most of the material in a real impact (as in the idealized one-dimensional case) the equation of state implies a direct relation between particle velocity and shock pressure. McSween (1985) gives a comprehensive review of the SNC meteorites, including a description of several proposed ejection mechanisms. One of these is the Melosh (1984) model of impact spallation. We will address the predictions of this model for ejection velocity, fragment size, and extent of the lightly-shocked region at length below.

Another context in which spallation is of interest is the evolution of asteroids (and by implication planetesimals in the early solar system). Here we are concerned not with the production of a small quantity of exceptional ejecta, but with impacts under such low gravity that strength effects are important on a large scale. Not only will gravity be unimportant for craters with depths up to 50 m on the largest asteroids (Gaffney, 1978), but the likely low strength of the regolith on these bodies may lead to the escape of a substantial fraction of the ejecta (Cintala *et al.*, 1979). This process may be important in the evolution of asteroid families and belts (Capaccioni *et al., 1986)*. Finally, of course, impact spallation would be of intrinsic interest, regardless of its quantitative significance for the production of ejecta.

In the past spallation has been studied in near surface or surface explosion craters (Stump and Reinke, 1984). The physics of spallation in rocks has been modeled in detail by Curran *et al.* (1977) and Grady and Kipp (1980). Other evidence of the role of spallation in large impacts is the observation of lightly shocked ejecta originating from near the free surface of impacts modeled numerically by Ahrens and O'Keefe (1978). Vickery (1986) finds evidence for relatively high velocity spalls from analyses of lunar and Martian secondary craters, but concludes that large fragments could not escape by this mechanism from either the Moon or Mars. However, there are no published values of spall velocities measured from experimental impact events.

This paper will begin with a description of the spallation experiments and the results of the spall velocity measurements. A preliminary discussion of these results was given by Polanskey and Ahrens (1985). Next the Melosh (1984) model will be described in detail. This will include a discussion of the relationship between the proposed lightly shocked region of the target and internal fractures observed beneathe several of the impact craters. Vertical spall velocities predicted by the Melosh hydrodynamic ejection model will then be compared to the measured spall velocities.

EXPERIMENTAL PROCEDURES

The spall velocity experiments can be divided into two groups. In February 1984, preliminary spall velocity measurements were made at the Caltech shock wave laboratory for two low velocity impacts. The remaining experiments spanned a wide range of impact velocities and were conducted in September 1984 at the NASA Ames Vertical Gun Range. In all cases, the target material was San Marcos gabbro. This material has a density, ρ_t, of 2.9g/cm^3, longitudinal wave velocity, C_L, of 6.4km/sec, and a dynamic tensile strength, σ_t, of 0.15GPa as measured by Lange et al., (1984a). To the level of approximation used in this paper, C_L is considered to be independent of stress. Birch (1964) calculates the Poisson ratio, ν, for San Marcos gabbro as 0.37. A more complete characterization of this rock can be found in Lange *et al*. (1984b).

For the low velocity experiments a 30/06 rifle was used to obtain impact velocities near 1km/sec. The projectile for the first shot was a 4.1g lead bullet measuring 7.8mm in diameter and 2.4cm in length. For the second shot, a 7.9mm diameter aluminium sphere with a mass of 0.65g was chosen in order to reduce the density difference between the projectile and target. The target material was cut into blocks roughly 16cm on a side and mounted with concrete into sections of 27cm diameter PVC pipe. The total target mass was just under 30kg. The targets were mounted in a vacuum tank kept at atmospheric pressure and containing three He-Ne lasers to measure projectile velocity (Figure 1a). Two x-ray tubes were positioned approximately 1m outside of the tank (1.5m from the point of impact), and were timed to photograph both the target immediately before impact and the ejecta and spall fragments 300μsec later. The spall velocities were determined by measuring the distance traveled by the spall fragment from the rock surface and the time elapsed since impact (Figures 1b,c). The spall fragments appear to be ejected at an angle close to 90° from the target surface; however, at the time of the second x-ray exposure, the spalls had not yet completely separated from the target.

→ Fig 1
c
Table I

The projectiles for the Ames experiments were primarily 3.2mm diameter iron and aluminium spheres. Impact velocities ranged from 1.7km/sec with the powder gun to 6.5km/sec for the light gas gun. Projectile masses were between 1.06 and 0.04g (see Table I). The targets were 23 to 30kg unmounted blocks of San Marcos gabbro placed in a tank evacuated to 5mm Hg. The cratering events were recorded by a Dynafax model 350 35mm framing camera with framing rates between 9000 and 35,000frames/sec. Illumination was provided by a Cordin model 359 strobe. The photographic equipment was located outside of the vacuum tank approximately 1.5m from the point of impact. Figure 2 shows three frames taken from one of these films. These frames are separated by 2 msec and the positions of one prominent spall fragment are marked. After each shot the range of each spall fragment was also recorded (Figure 3a). Since spallation is a near surface phenomenon, for these measurements a spall fragment was defined as any piece of ejecta containing part of the original top surface of the target. Later each spall fragment was weighed and its thickness from the top surface to the maximum depth was measured (Figure 3b).

Fig 2
Fig 3

Crater volumes were determined by measuring the volume of dry #120 Ottawa sand required to fill them. Finally, three of the targets were bisected through the center of the crater in order to observe the internal fractures. The results of the fracture analysis will be presented later in the Discussion section.

RESULTS

In all cases, the craters consisted of two distinct zones. The lower central pit region was highly fractured and covered with finely crushed rock, while the wide outer spalled region was shallow, with a relatively clean surface. In several cases the plan view of the outer perimeter was very irregular. There is also evidence of incomplete spalls which were either only partially separated from the target or just visible as cracks on the surface. All of these features are consistent with other reports of cratering into competent rock targets (Lange *et al.*, 1984b; Moore *et al.*, 1963; Horz, 1969). However, other aspects of the targets will be described later. The measured crater volumes are plotted as a function of projectile energy in Figure 4 to show the good agreement between the present targets and earlier cratering experiments .

Fig 4

Analysis of the x-ray records from the two low velocity shots give vertical spall velocity measurements of 11m/sec and 17m/sec for the lead and aluminium projectiles, respectively. These velocities are both less than 2% of the impact velocity. Some vertical spall velocity measurements were made for the Ames shots from the framing camera films. However, as evident in Figure 2, it is difficult to distinguish the spall fragments from the other ejecta. This was partially due to a malfunction in the strobe system which resulted in underexposed films. The spall velocities measured ranged between 7 and 27m/sec with large variations in velocity within each event. Variations in velocity with time were also observed for individual spall fragments. This may be partly a consequence of the spinning and tumbling of the fragments in flight. Ejection angles could not be measured directly from the two-dimensional films, and attempts to determine ejection angle by correlating the spalls observed on the films with those located after the event proved to be unreliable. Also, in some cases the spalls were observed to fragment in flight. However, it is unclear if this was actually fragmentation, or merely an effect due to the poor resolution of the films.

Fig 5

Due to these complications of measuring velocities from the Ames films, estimates of spall velocity were made from the measured range data. This was done by a simple application of the ballistic equations of motion. Although an ejection angle is needed for such a calculation, it can be shown (Figure 5) that the velocity is relatively insensitive to variations in angle between 20° and 55°, measured from the horizontal. Therefore, a simple assumption of a 45° ejection angle was used to calculate the minimum spall velocity needed to satisfy the range data. This angle is also compatible with the 42° asymptotic ejection angle given by Melosh (1984) for a target material with $\nu = 0.4$. He finds that the ejection angle decreases from near vertical to the asymptotic ejection angle with increasing distance from the point of impact. The resulting minimum velocities are plotted in Figure 6 along with the velocities measured from the films. Note in that the velocities measured from the films are up to an order of magnitude higher than the indirectly calculated velocities. The difference between the two measurements cannot be solely the result of the chosen ejection angle, because even increasing the angle to 80° would only effectively double the ejection velocity. However, this velocity difference is minor when compared its difference from the impact velocity.

Fig 6

The measured spall masses and thicknesses were then compared with the range measurements (or equivalently, the minimum spall velocity). As shown in Figure 3, there is no simple correlation of spall mass or thickness with range. This observation was verified by fitting the data set for each shot using linear least squares. The highest correlation coefficient obtained was only 0.24 for shot 840904, and the remaining shots had substantially lower correlations.

DISCUSSION

Melosh (1984) derives two models based on the concept that the stress waves from an impact event are similar to those of an explosive source buried at some depth. First a hydrodynamic ejection model is presented using the interaction between a compressive wave and the corresponding tensile wave relected from the target's free surface to predict spall velocities and thicknesses. Next, a stress wave ejection model is devoloped by adding the effect of a reflected shear wave to calculate ejection angles and fragment sizes. Fragment size is predicted to be inversely proportional to ejection velocity, and ejection angle is found to be a function of the target tensile strength and Poisson ratio. Although Melosh concludes that spallation is an unlikely mechanism for removing significant quantities of material from the Martian surface, it is potentially an important process for ejecting material from asteroids and possibly the Moon.

In order the explain the application of the Melosh model to the present experiments, we first briefly review the relevant aspects of Melosh (1984) with emphasis on the hydrodynamic ejection model. One important feature of the model is that there exists a region, the near surface zone, where the target material experiences reduced compressive stress as a consequence of its proximity to a free surface. To satisfy the free surface boundary condition of zero stress, the compressive wave generated by the buried source is exactly canceled at the surface by the reflection of a tensile wave of equal magnitude. It then follows that below the surface the two waves will superimpose by virtue of their finite rise and decay times. The near surface zone is the region where the delay between the two waves is less than the rise time of the compressive wave. This region never sees the peak of the compressive stress pulse, and is therefore the proposed source of the lightly shocked ejecta.

The depth of the near surface zone is strongly controlled by the shape of the stress pulse. The pulse shape will be characterized by a rise time, τ, and a decay time, τ_D where τ is generally less than τ_D. For an impact, τ is modeled as a/U, where a is the projectile radius, and U is the impact velocity. In this model the rise time is taken to remain constant as the shock propagates, although this may not be strictly true for small scale impacts (Melosh,1984). The depth of the near surface zone boundary is defined by the hyperbola:

$$Z_p = \frac{C_L\tau}{2}\left(\frac{4(d^2 + s^2) - C_L{}^2\tau^2}{4d^2 - C_L{}^2\tau^2}\right)^{1/2} \qquad (1)$$

where $d=2a(\rho_p/\rho_t)^{1/2}$ is the equivalent depth of burst for a projectile density ρ_p, and s is measured from the point of impact along the target surface (Melosh, 1984). Figure 7 illustrates the relationships between s, d, and Z_P for the experimental conditions of shot 840904.

Fig 7

Physical evidence for the existence of the near surface zone was suggested by the distribution of fractures observed when three of the targets were bisected. The visible fractures fall into three major catagories in two different areas of the target. First, there is a hemispherical region of closely spaced radial fractures immediately surrounding the crater and extending outwards for at least 10 projectile diameters. Within this region are also larger circular fractures concentric around the point of impact. Secondly, subhorizontal fractures are found below and parallel to the floor of the spalled zone. These fractures resemble those observed by Maurer and Rinehart, (1960) in several targets from very low velocity experimental impacts.

Outside the radially fractured region there are relatively few other visible fractures. Those few, however, constitute a third well-defined category: a set of major cracks forming a conspicuous pattern closely resembling the boundary of the near surface zone as defined by Equation (1). It is also interesting to note that no cracks were found above this region. A straightforward calculation of Z_p for the relevant experimental parameters gives a remarkable fit of the near surface zone boundary to the actual cracks observed in the two high velocity experiments (Figure 8a,b).

Fig 8

The target for the low velocity shot 603 was qualitatively similar to those described above, although the radially fractured zone was significantly smaller. The most obvious feature in this target was one large crack beginning at the floor of the crater and extending in an arc to a depth of 6cm. Although this crack had the same general form as the Z_p boundary, it was assymmetric and did not match the curve defined by the parameters for that experiment. This is not unreasonable since the projectile was a commercial bullet having a high density and a nonspherical shape. Determining the rise time of the stress wave from the geometry of the bullet iss not straightforward. The curve in Figure 8c was fit to this fracture by specifying the values of a and d to be 0.28cm and 1.5cm, respectively. This value for a, however, gives a rise time 28% less than that based on the bullet radius. Also, this depth of burst falls below the crater floor and is slighlty greater than it would be if it were calculated with a 0.28cm projectile radius. However, manipulating the equations to fit the fracture from this shot is not as important as recognizing its qualitative resemblence to the fractures in the two other targets.

The only other fractures visible in the three targets were those located close to and parallel to the vertical sides of the blocks. These cracks were presumably due to boundary effects. The same wave interaction should occur at the sides of the target as it does at the top surface, and a near surface zone could be calculated as well. However, the resulting boundary curve is much flatter and closer to the target surface. An example of this curve is plotted for shot 840906 in Figure 8b; however, the boundary does not correlate with the vertical fractures observed.

Returning to the Melosh hydrodynamic ejection model, we consider its predictions for spall thicknesses and velocities as a function of s and z. The spall thickness, defined as the depth at which the tensile stress reaches the dynamic tensile strength of the target material, is given by Melosh (1984):

$$Z_S = \frac{\sigma_t}{P(r_0)} \frac{\tau_D C_L}{2d} \frac{r_0}{(1 - 1.87\tau_D C_L/r_0)} \qquad (2)$$

where $\tau_D = d/C_L$, $P(r_0) = \rho_t C_L \upsilon_p(r_0)$ is the pressure for a particle velocity $\upsilon_p(r) = (U/2)(\rho_p/\rho_t)(a/r)^{1.87}$, and r and r_0 are distances illustrated in Figure 7. This equation for Z_S is valid only for z above the Z_p boundary. The empirical quantity -1.87 comes from the exponent of pressure decay adopted by Melosh for the stress pulse. Recent calculations by Ahrens and O'Keefe (1986) find this decay exponent to vary with impact velocity. Their results predict a pressure decay exponent of -1.87 for the impact of a silicate projectile on a silicate target at 9.8 km/sec. The relationship between Z_P and Z_S is shown in Figure 8a,b. It is interesting to note that, in agreement with the Melosh model, Z_S intersects the Z_p curve at the edge of the observed crater.

Next, the spall velocity is given for any r within the near surface region as (Melosh, 1984):

$$\upsilon_{V|\mathrm{spall}} = \frac{2\upsilon_P(r)d}{r_0}\left(1 - \frac{2d}{r_0}\,\frac{Z_S}{C_L\tau}\right). \tag{3}$$

One basic assumption of this model is that the spall thickness is much smaller than all other dimensions. When this is true, the second term in the parentheses is negligible, and the spall velocity approaches the maximum value, $\upsilon_{max} = 2\upsilon_P(r)d/r_0$. The spall thickness term can be neglected for large planetary scale impacts; but is, however, quite large in the models of the laboratory scale impacts. The correction term varies from 0.38 to beyond the limit of 1.0 for the present experiments. Therefore, the predicted velocities for the laboratory impacts can be at most 62% of the maximum spall velocity. It must also be noted that Equations (2) and (3) are not valid for s less than approximately four projectile radii from the point of impact. For small s, Z_S becomes negative as a result of certain approximations in the model. This will have important implications later in our paper.

Although $\upsilon_{V|\mathrm{spall}}$ is a function of both s and z, the calculated spall velocities in Figure 9 are the results of the Melosh model applied to the laboratory shots for the limiting case of z = 0. This represents the maximum velocity possible at any given s. The appropriate experimental values of U, a, and ρ_P were used with Equation (3) to generate each curve in Figure 9. The steep decrease in velocity towards the center of the crater is a result of Z_S becoming negative at small s. This portion of the curve can be neglected. Shaded rectangles are included on each plot to compare the model results with the experimental results. The vertical sides of each rectangle represent the range of spall velocities measured experimentally. The horizontal sides of the rectangles limit the range of s to the spalled region measured from each of the craters (Figure 7). In all of the Ames experiments the model velocity curves intersect the measured velocity fields. Generally, the measured velocities agree with the lower limits of the model; however, these curves do represent the maximum velocity at any distance along the surface. Furthermore, the model predicts a strong decrease of spall velocity with depth. Since each spall fragment has a finite thickness, its average velocity would be lower than that predicted for a point on the surface. Therefore,the present results compare well with the Melosh model, despite the fact that these equations were formulated for conditions much different than those found in small-scale laboratory impacts.

Fig 9

The effect of this scale difference becomes more severe at low impact velocities. Equations (2) and (3) are difficult to apply to shots 603 and 608, because the projectile radius is quite large compared to the resulting crater. Thus the depth of burst calculated according to the above formula is also greater than the actual crater depth. Nevertheless, for these shots rough estimates of spall velocity were calculated for Figure 9 by adjusting d to equal the depth of the crater. In the case of shot 603, this d turns out to be above the depth of burst determined earlier when fitting the Z_p curve to the large fracture.

The Ames experiments are more similar to the conditions described by the Melosh model, because higher impact velocities lead to the strong stress waves needed to satisfy the hydrodynamic approximations. In addition, the projectile radii were smaller which, combined with higher impact velocities, gave shorter rise times. This is desirable because the approximations also require that r be greater than $C_L\tau$. Therefore Equations (2) and (3) could be applied throughout a greater fraction of the crater volume. Nevertheless, the assumption that spall thicknesses are much smaller than the projectile radius has been violated in most cases.

SUMMARY AND CONCLUSIONS

Analysis of the interior of three targets revealed the absence of visible fractures above the predicted boundary of the near surface zone. Furthermore, in the two high velocity experiments the theoretical Z_p boundary could be linked to definite fractures observed in the targets. This correlation gives physical support to the model, and indicates that the material above this boundary may be less highly shocked than target material at a similar radial distance below the crater floor.

Both the spall velocities measured from the films and those determined from the range measurements are consistent with the vertical spall velocities predicted by the Melosh hydrodynamic model. This statement is valid despite the assumptions inherent in the model which restrict its application to laboratory impacts. The spall velocities measured were all less than a few percent of the respective impact velocities. The greatest spall velocity measured, 27m/sec, was for shot 840904 and was only 0.5% of the 5.4 km/sec impact velocity. Scaling this measured spall velocity to that expected for a large impact is difficult if using only the equations presented in the above discussion. One simple approach is to examine the basic functional dependencies of Equation (3) We see that spall velocities are primarily a function of impact velocity and the distance from the impact point normalized to the projectile radius. This suggests that spall velocities resulting from the impact of an asteroid traveling at 5km/sec would directly scale with s/a to those velocities measured experimentally.

Neglecting the effects of a regolith, the 27m/sec spall velocity would enable fragments to escape only parent asteroids less than 46 km in diameter. While this would include objects such as Phobos or Diemos, it would exclude the presumably igneous differentiated asteroids such as Ceres and Vesta.

However, the more detailed stress wave ejection model for impacts of larger bodies permits the possibility of high speed fragments not observed in the present experiments or calculations. This model, unlike Equation (3), does not suffer from the restriction that the fragments must originate from regions farther than four projectile radii from the point of impact. Melosh (1986) provides a plot of spall velocities as a function of depth for s between one and five projectile radii. The results predict spall velocities in excess of 13% of the impact velocity for s/a less than 1.4. For the present experimental impacts, the projectile radii are as small as 0.159 cm. Therefore, if these high velocity spalls exist, they could not be observed on the films. Even for large impacts, the high velocity fragments would be a small fraction of the spall fragments ejected. Using this argument, Melosh predicts spalls capable of escaping the Moon but not Mars. However, the present results support the Melosh velocity model only at its lower limits where the spall fragments are large enough to be observed.

ACKNOWLEGDEMENTS

I wish to thank Dr. Jay Melosh for helpful technical discussions and Dr. Peter Schultz for his assistance in utilizing the Ames facility. This research was supported by NASA Grant NGL-05-002-105. Contribution no. 4405, Division of Geological and Planetary Sciences, California Institute of Technology, Pasadena, California.

REFERENCES

AHRENS, T. J. and J. D. O'KEEFE (1986). Impact on the Earth, ocean, and atmosphere. *Proc. 1986 Hypervelocity Impact Symp., In Int. J. Impact Engineering*, **5**, in press.

AHRENS, T. J. and J. D. O'KEEFE (1978). Energy and mass distributions of impact ejecta blankets on the Moon and Mercury. *Proc. Lunar Planet. Sci. Conf. 9th*, 3787-3802.

BIRCH, F.(1966). Compressibility; Elastic constants. In *Handbook of Physical Constants* (S. Clark, Jr. Ed.), Geol. Soc. America Memoir 97, 97-173.

CAPACCIONI, F., P. CERRONI, M. CORADINI, M. DI MARTINO, P. FARINELLA, E. FLAMINI, G. MARTELLI, P. PAOLICCHI, P.N. SMITH, A. WOODWARD, AND V. ZAPPALA (1986). Asteroidal catastrophic collisions simulated by hypervelocity impact experiments. *Icarus* 66, 487-514.

CINTALA, M. J., J. W. HEAD, and L. WILSON (1979) The nature and effects of impact cratering on small bodies. In *Asteroids* (T. Gehrels, Ed.), pp. 579-600. Univ. of Arizona Press, Tuscon.

CURRAN, D. R., D. A. SHOCKEY, L. SEAMAN, and M. AUSTIN (1977). Mechanisms and models of cratering in earth media. In *Impact and Explosion Cratering* (D. J. Roddy, R. O. Pepin, and R. B. Merrill, Eds.), pp. 1057-1087. Pergamon Press, New York.

GAFFNEY, E. S. (1978). Effects of gravity on explosion craters. *Proc. Lunar Planet. Sci. Conf. 9th*, 3831-3842.

GRADY, D. E. and M. E. KIPP (1980). Continuum modeling of explosive fracture in oil shale. *Int. J. Rock Mech. Min. Sci. & Geomech. Abstr.* 17, 147-157.

HORZ, F. (1969). Structural and mineralogical evaluation of an experimentally produced crater in granite. *Contrib. Min. Petrol.* 21, 265-277.

LANGE, M. A., T. J. AHRENS, and M. B. BOSLOUGH (1984a). Cratering and spall fracture in gabbro. Chapter XI:7, *Shock Waves in Condensed Matter 1983* (J. R. Asay, R. A. Graham, and G. K. Straub, Eds.),pp.525-528. Elsevier Science Publishers B.V.

LANGE, M. A., T. J. AHRENS, and M. B. BOSLOUGH (1984b). Impact cratering and spall failure of gabbro. *Icarus* 58, 383-395.

MAURER, W. C. and J. S. RINEHART (1960). Impact crater formation in rock. *J. Appl. Phys.* 31, 1247-1252.

MCSWEEN, H. Y. (1985). SNC Meteorites: Clues to Martian petrologic environment? *Rev. Geophys.* 23, 391-416.

MCSWEEN, H. Y. and E. STOLPER (1980). Basaltic meteorites. *Sci. Amer.* 242, 54-63.

MELOSH, H. J. (1986). High-velocity solid ejecta fragments from hypervelocity impacts. *Proc. 1986 Hypervelocity Impact Symp., In Int. J. Impact Engineering*, 5, in press.

MELOSH, H. J. (1984). Impact ejection, spallation, and the origin of meteorites. *Icarus* 59, 234-260.

MOORE, H. J., D. E. GAULT, and R. V. LUGN (1963). Experimental impact craters in basalt. *Trans Soc. Mining Engineers* 226, 258-262.

O'KEEFE, J. D. and T. J. AHRENS (1985). Impact and explosion crater ejecta, fragment size, and velocity. *Icarus* 62, 328-338.

POLANSKEY, C. A. and T. J. AHRENS (1985). Spall velocity measurements of laboratory scale impact craters (abstract). *In Lunar and Planetary Science XVI*,pp.671-672. The Lunar and Planetary Institute, Houston.

STUMP, B. W. and R. E. REINKE (1984). Spall observations and mechanisms in alluvium. *J. Geophys. Rev.* 89, 11,495-11,506.

VICKERY, A. M. (1986) Size-velocity distribution of large ejecta fragments. *Icarus* 67, 224-236.

WOOD, C. A. and L. D. ASHWAL (1981). SNC meteorites: Igneous rocks from Mars. *Proc. Lunar Planet. Sci.* 12B, 1359-1375.

TABLE I.

Experimental parameters and crater characteristics

Shot	Target	Projectile				Crater		
Number	Mass	Type	Mass	Radius	Velocity	Depth	Diameter	Volume
	(kg)		(g)	(cm)	(km/sec)	(cm)	(cm)	(cm^3)
603	23	Pb	4.10	0.391	0.89	0.95	6.3	9.5
608	23	Al	0.65	0.397	1.01	0.35	2.2	<0.5
840901	24	Al	0.0443	0.159	6.49	1.0	6.5	9.0
840902	25	Fe	0.1292	0.159	4.60	1.50	9.8	30.0
840904	29	Fe	0.1297	0.159	5.44	1.65	10.5	36.0
840905	23	Fe	0.1297	0.159	4.60	1.45	8.0	19.0
840906	13	Fe	0.1297	0.159	4.76	1.40	9.2	23.0
840907	23	basalt	0.1557	0.238	2.26	0.70	3.5	2.3
840909	24	Steel	1.0571	0.318	1.69	1.40	8.3	25.5

POLANSKEY AND AHRENS

FIGURE CAPTIONS

Figure 1. a) Sketch of experimental configuration for spall velocity measurements. The projectile velocity is determined by a counter measuring time intervals as the projectile breaks the laser beams. The lasers also activate other counters which then trigger the X-ray tubes. b) The first X-ray exposure is taken immediately before impact and shows the projectile in flight. c) The second exposure is taken approximately 300µsec later. Spall velocities can be measured directly from this exposure. In addition to the spalls, high speed ejecta and projectile fragments are also visible.

Figure 2. Three frames from shot 840904 are shown to illustrate the film coverage of the Ames experiments. The time above each frame is given with respect to the moment of impact, and the time lapse between frames is 2 msec. The spall fragment indicated by the arrows is traveling at approximately 7 m/sec. The outline of the targets has been retouched, and a scale is provided below the photographs for reference.

Figure 3. Combined results of measured spall range versus, a) spall mass and b) spall thickness for six of the Ames experiments. Aside from a few very large, low velocity spalls, there is no apparent correlation between either spall mass or thickness and range.

Figure 4. The current results of crater volume versus projectile kinetic energy are plotted along with data from previous cratering experiments on rock targets.

Figure 5. The calculated variation of spall velocity with ejection angle for a typical spall range measurement. Note that the curve is relatively flat for angles between 20° and 55°, varying in velocity by only 8%. The spall fragment used in this example had a mass of 2.6g and landed 52.1cm from the point of impact.

Figure 6. Combined results of the spall velocity experiments using both measurements from films (solid symbols) and calculations using the final spall range data and assuming an ejection angle of 45°.

Figure 7. Sketch of an experimental crater profile adapted from Melosh (1984). The relationships between the geometrical quantities s, z, r, r_0, and d are shown in relation to the crater depth profile from shot 840904. Also shown is an example of the range of s values, s_{min} to s_{max}, considered applicable for calculating spall velocities for this impact.

Figure 8. Sketches of the fractures found inside three of the gabbro targets. The shaded area indicates the highly fractured region immediately surrounding each crater. Plots of Z_p, the theoretical near surface zone (dashed line), are superimposed over the fractures. For shots 840904 and 840906, the calculated spall thickness, Z_s, is plotted (dotted line) within the near surface zone. The symbol below the surface of each target at $s = 0$ marks the equivalent depth of burst, d, used to calculate the curves.

Figure 9. Vertical spall velocity, as calculated from the Melosh equations evaluated at $z=0$, is plotted as a function of s to model each of the experimental impacts. The shaded rectangles provide a comparison of the experimental results to the model curves. The range of measured spall velocities for each event is indicated by the height of the rectangles. The horizontal extent of the rectangles represents the range

of s, s_{min} to s_{max}, measured from the spalled zone of each crater (as illustrated in Figure 3).

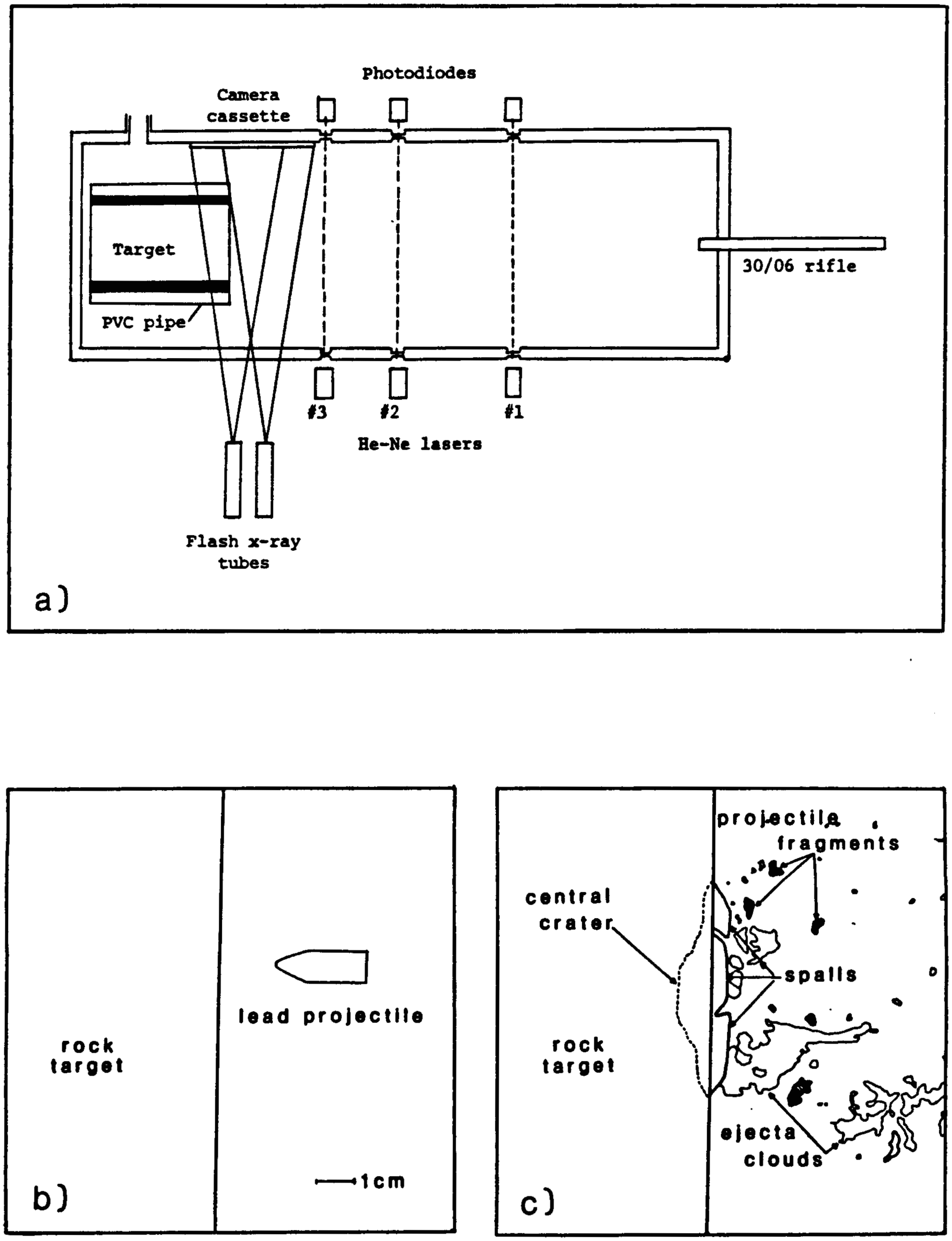

Fig 1 Polanskey and Ahrens

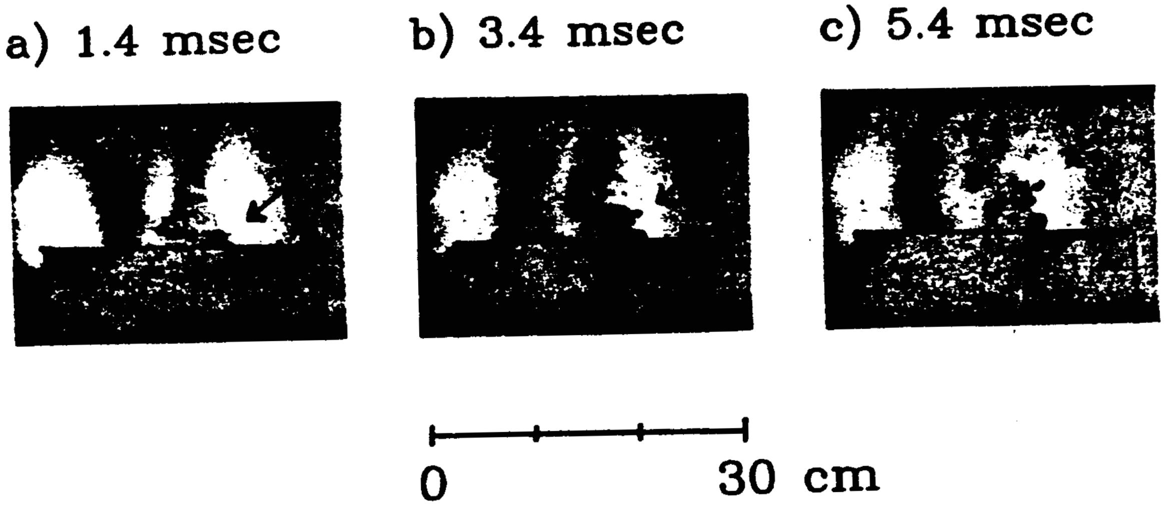

a) 1.4 msec

b) 3.4 msec

c) 5.4 msec

ORIGINAL PAGE
BLACK AND WHITE PHOTOGRAPH

FIG 2 POLANSKEY AND AHRENS

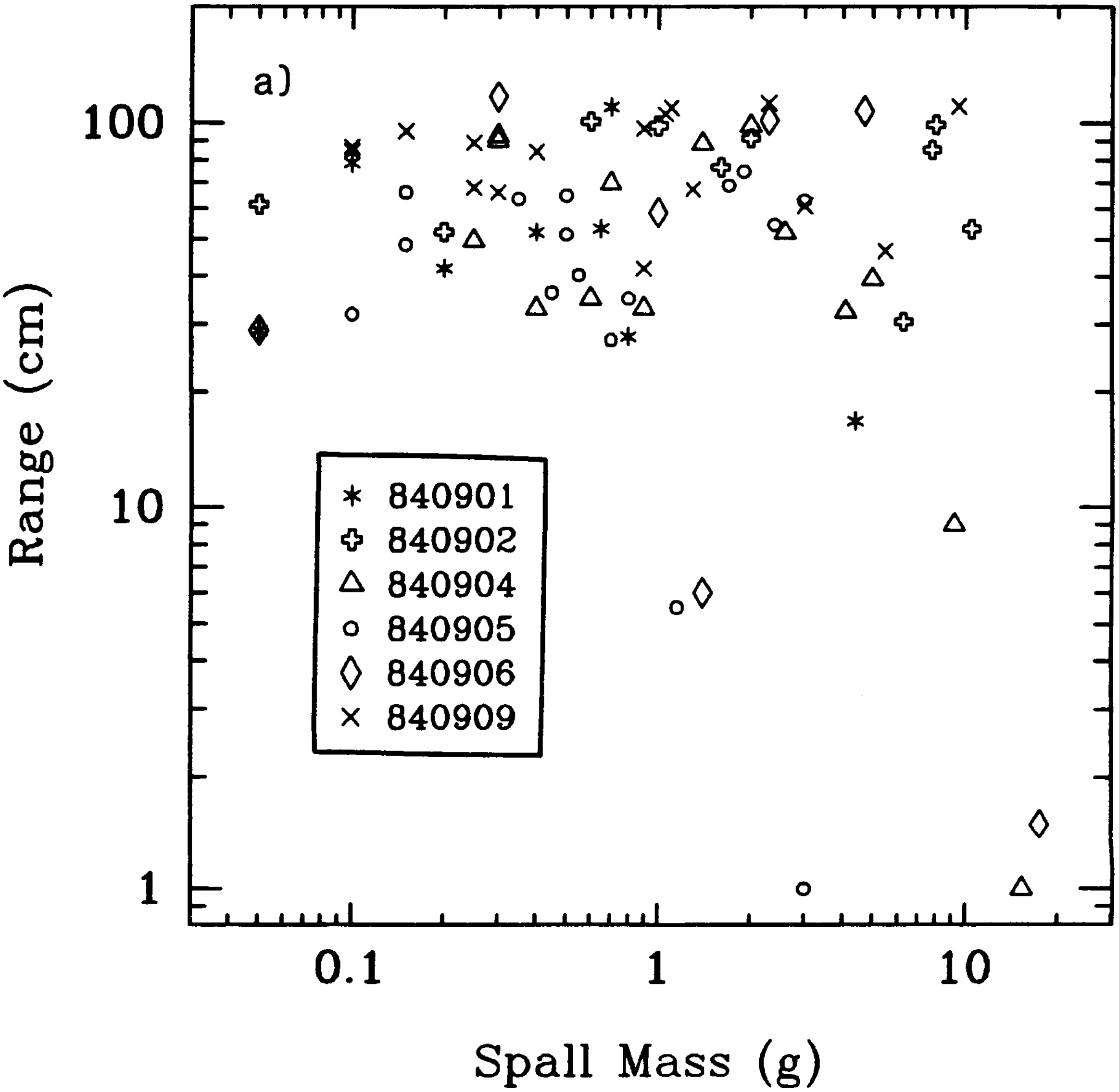

FIG 3a POLANSKEY AND AHRENS

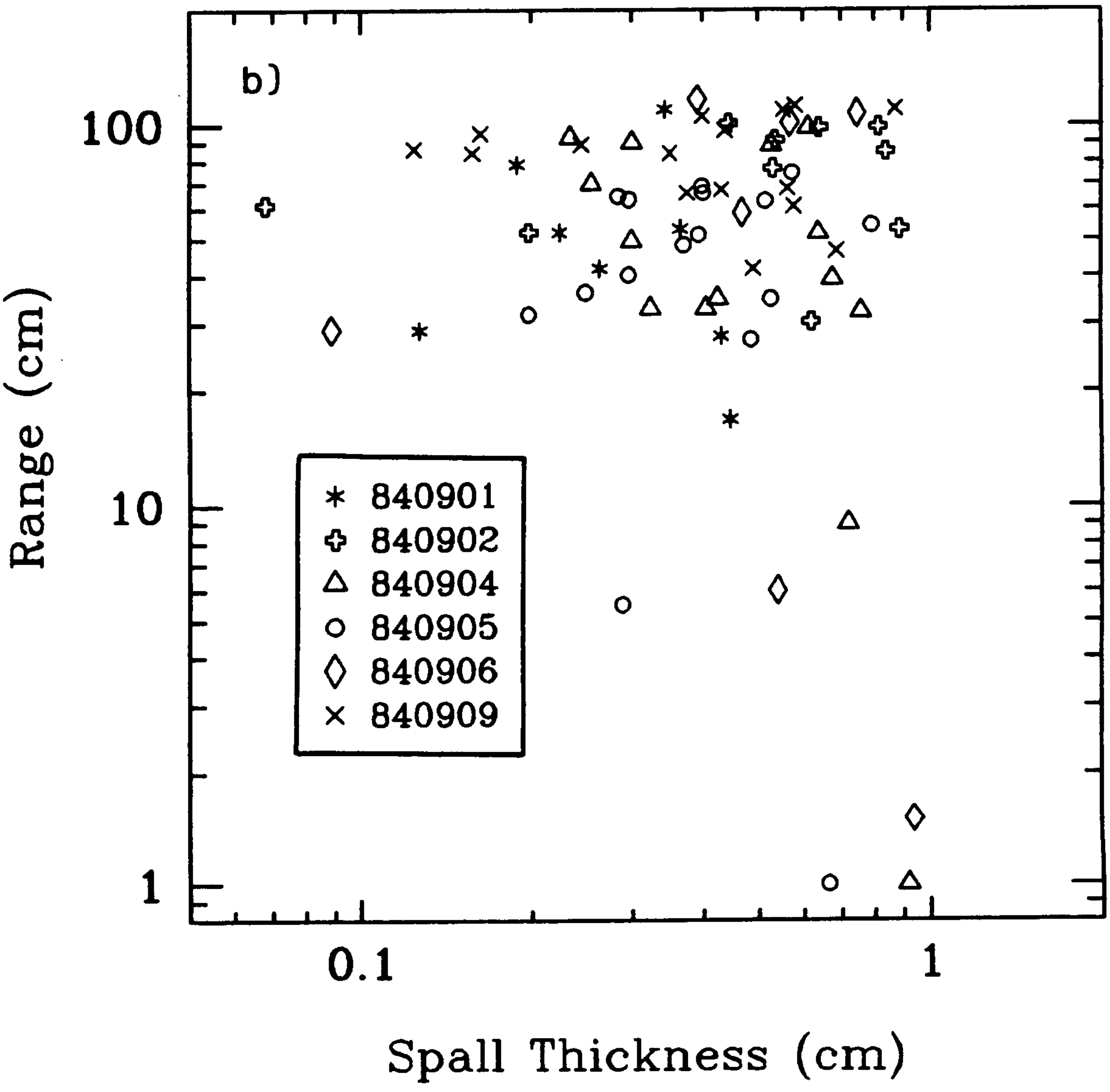

Fig 3b POLANSKEY AND AHRENS

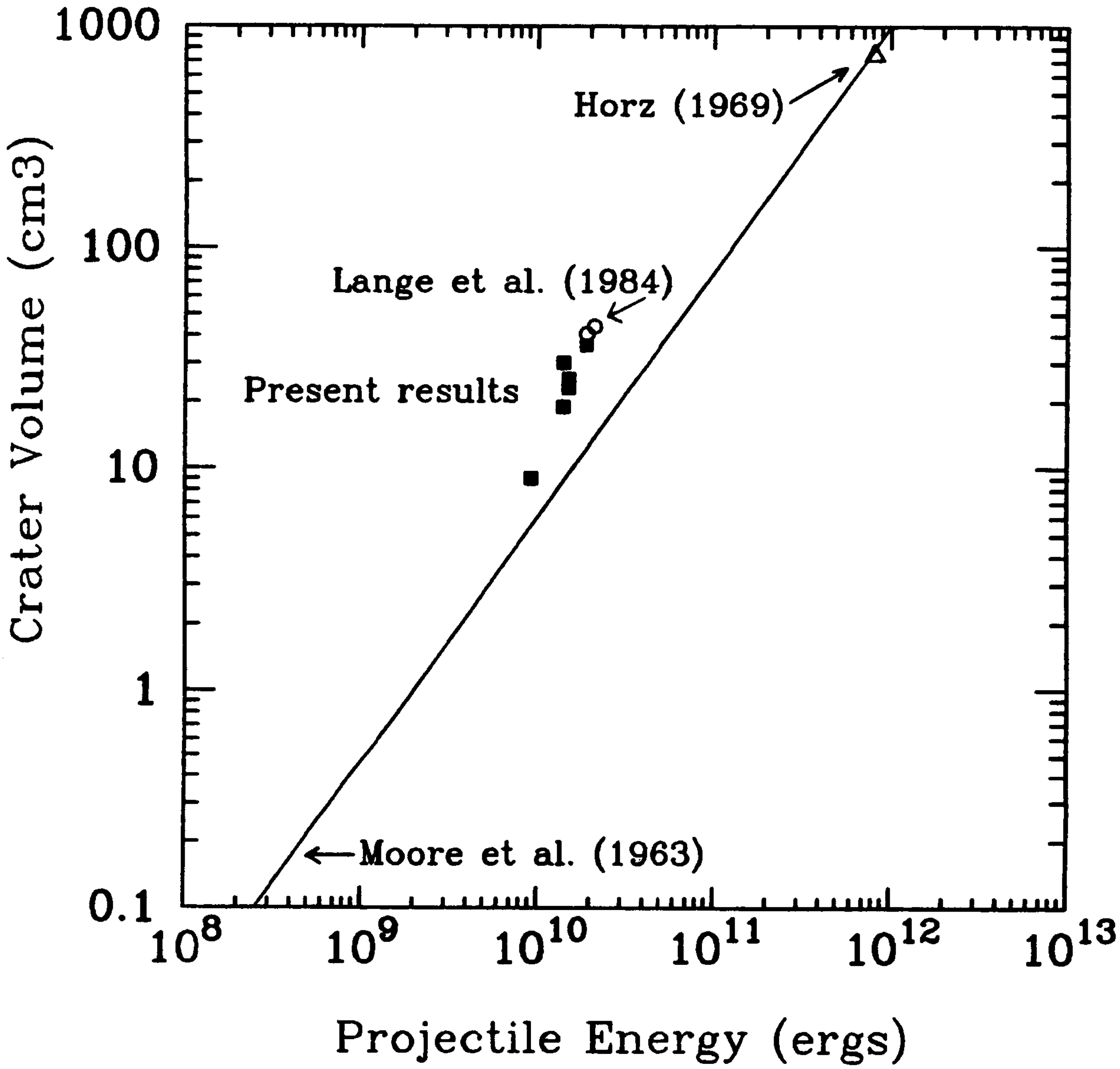

FIG 4 POLANSKEY AND AHRENS

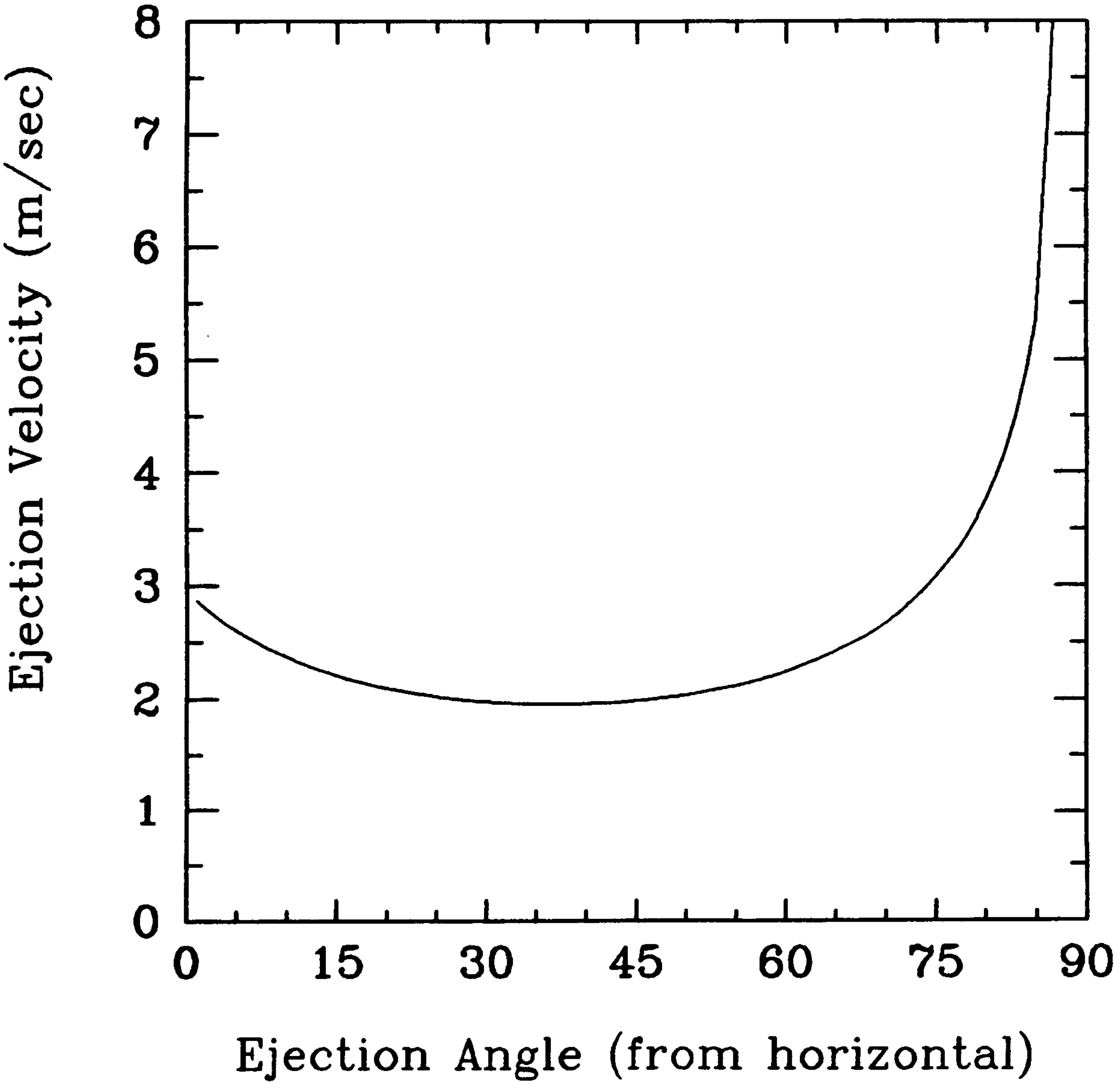

FIG 5 POLANSKEY AND AHRENS

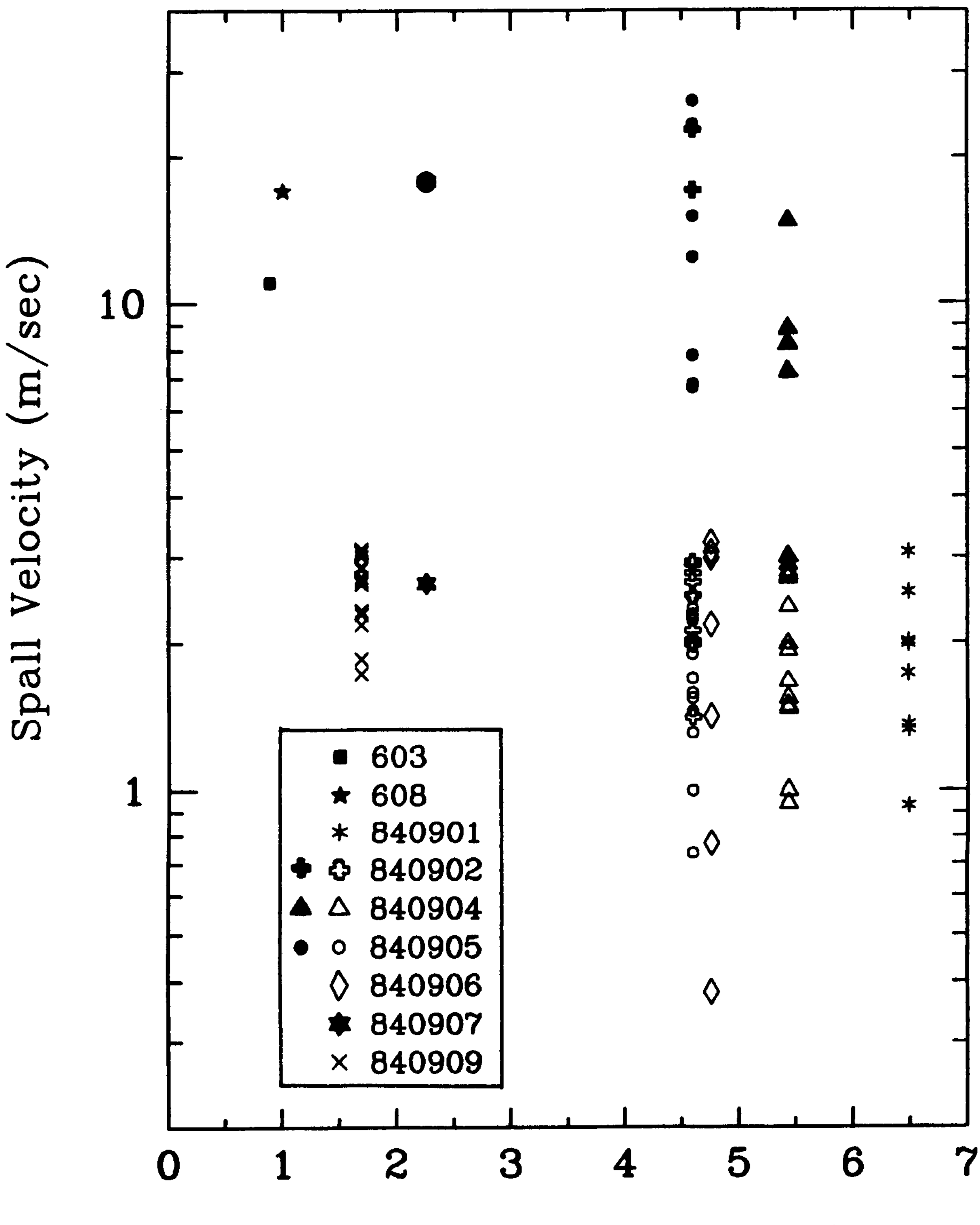

Fig 6 Polanskey and Ahrens

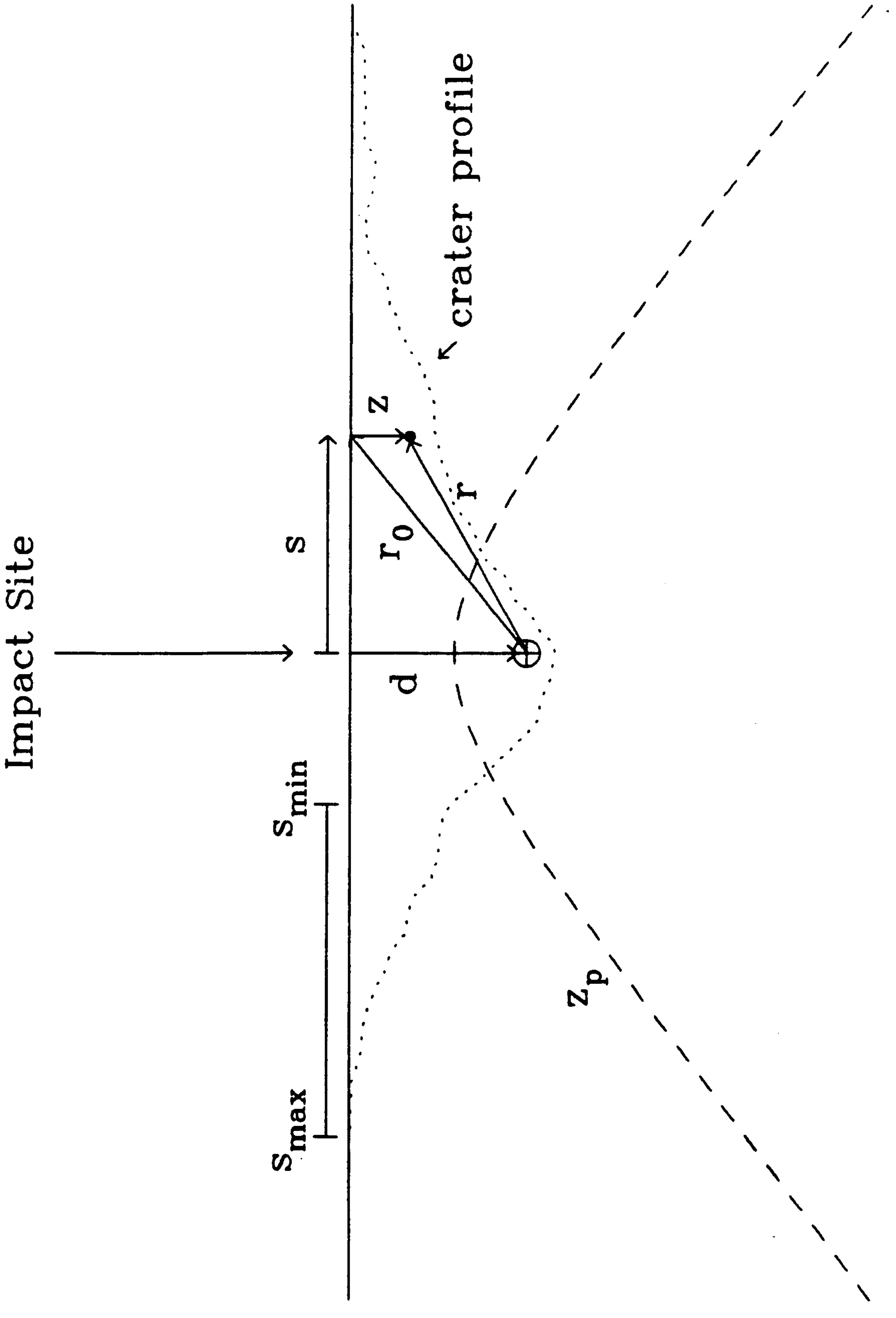

FIG 7 POLANSKEY AND AHRENS

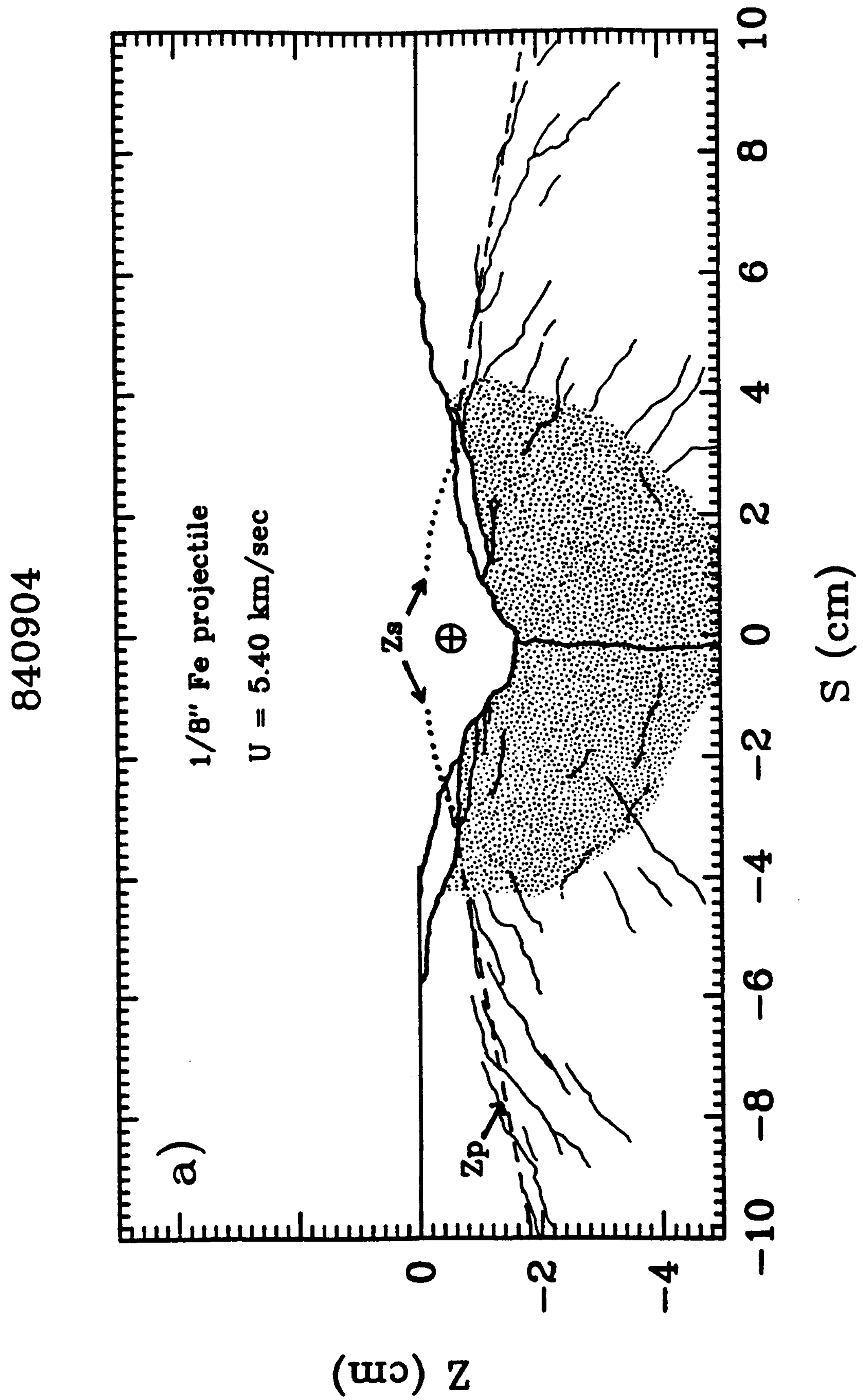

FIG 8a POLANSKEY AND AHRENS

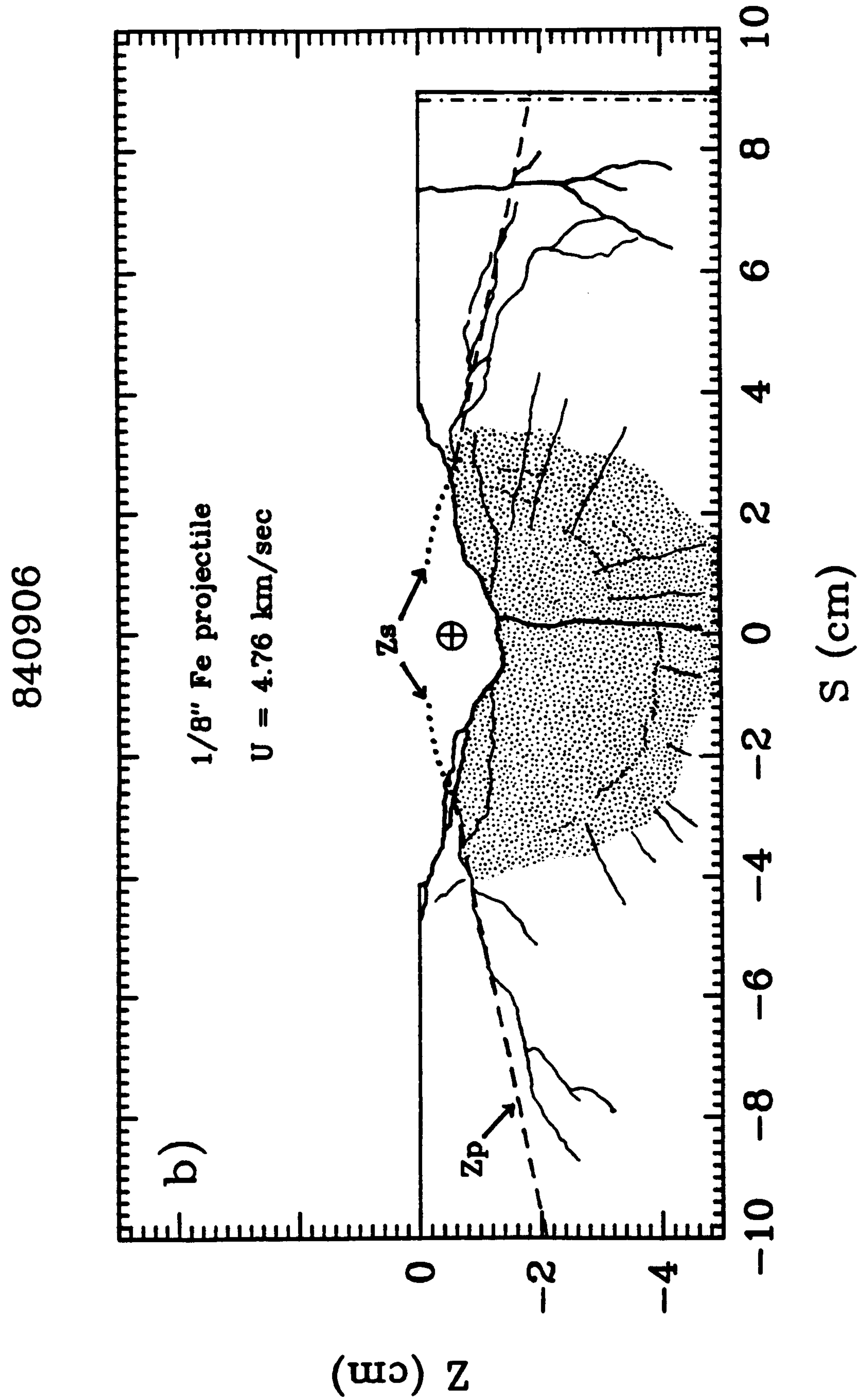

Fig 8b Polanskey and Ahrens

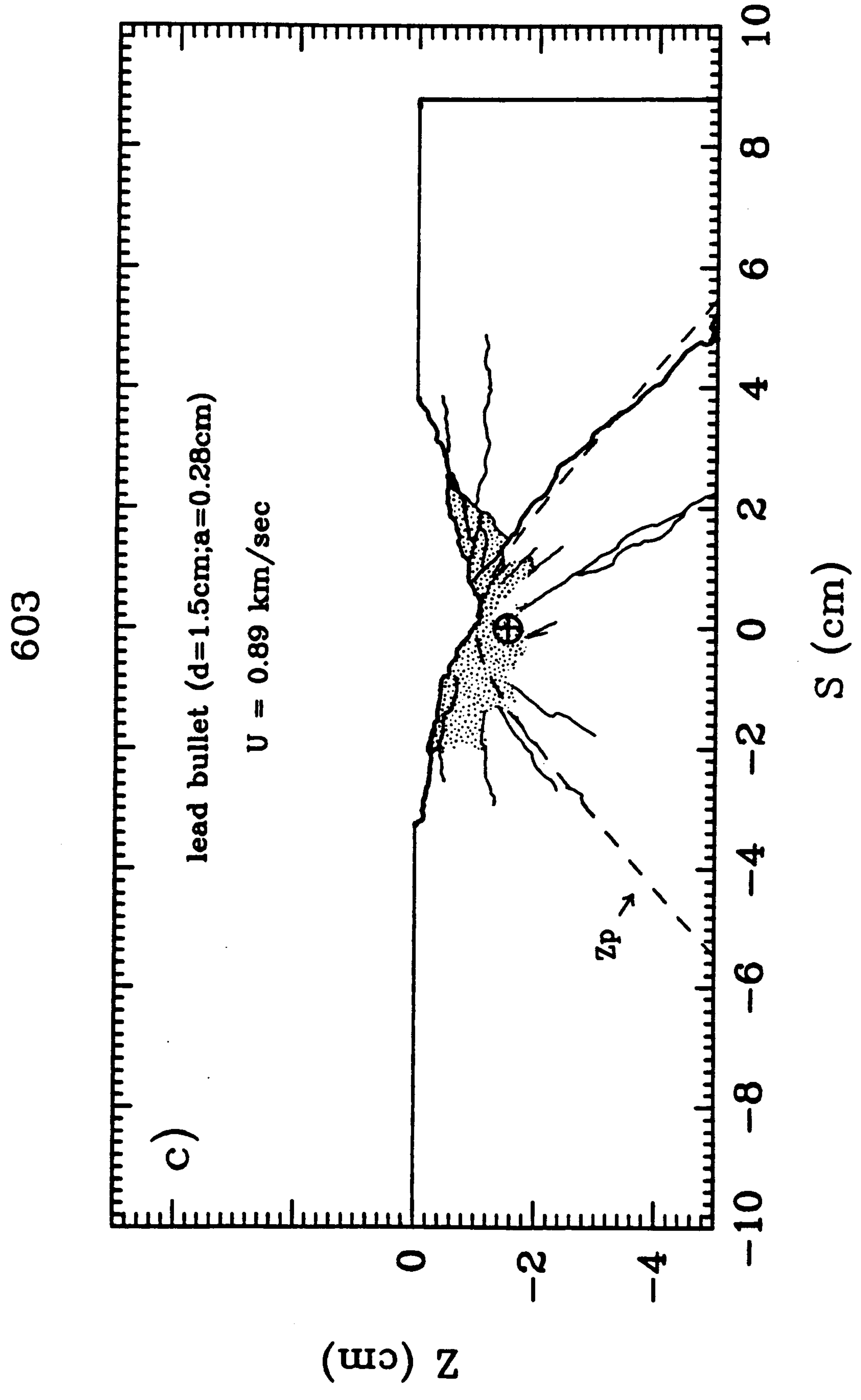

FIG 8C POLANSKEY AND AHRENS

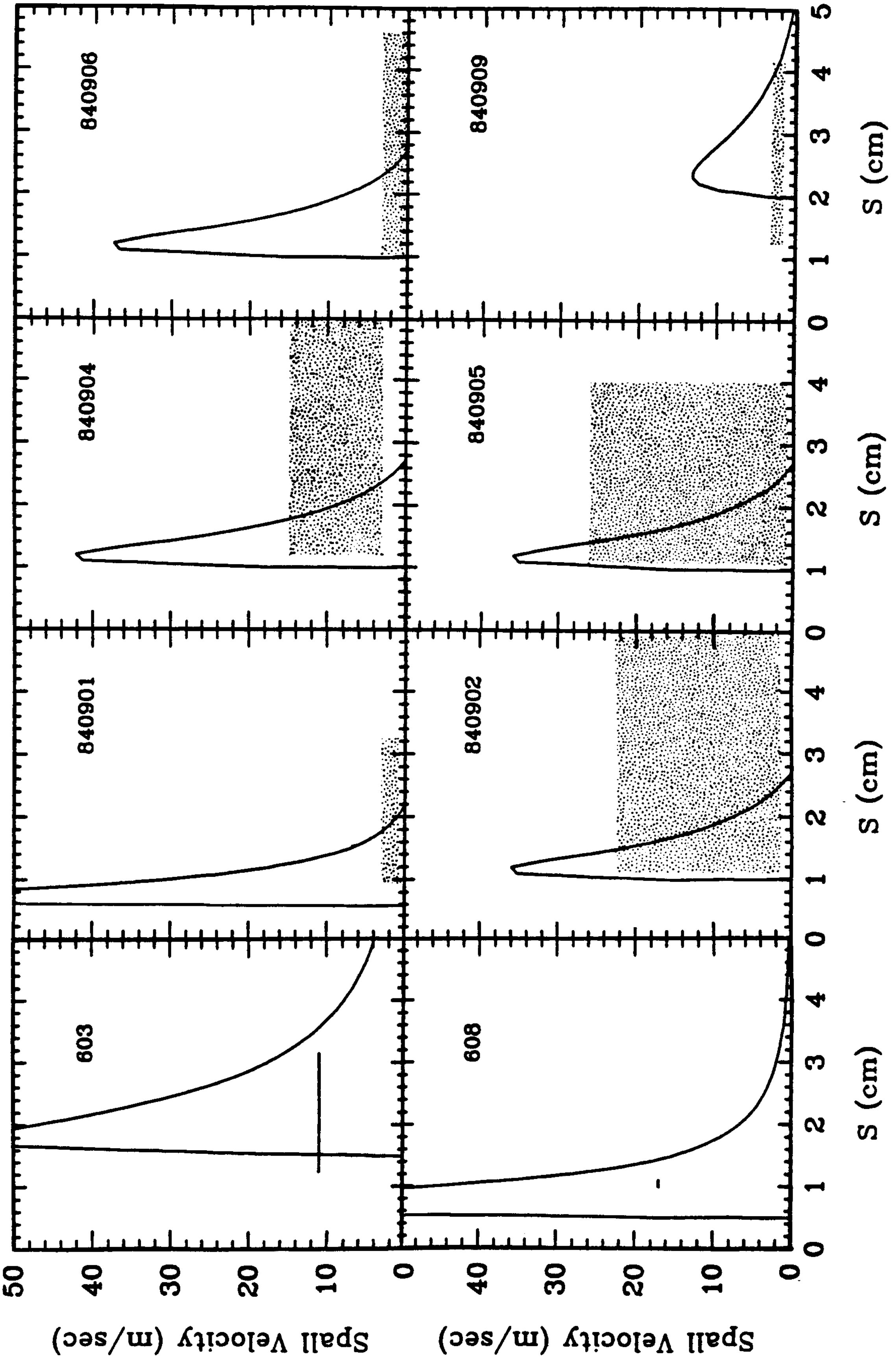

FIG 9 POLANSKEY AND AHRENS